Potential Energy Surface of Methanol Decomposition on Cu(110)

Donghai Mei,*,† Lijun Xu,‡ and Graeme Henkelman‡

Institute for Interfacial Catalysis, Pacific Northwest National Laboratory, Richland, Washington 99352, and Department of Chemistry and Biochemistry, University of Texas at Austin, Austin, Texas 78712

Combining the dimer saddle point searching method and periodic density functional theory calculations, the potential energy surface of methanol decomposition on Cu(110) has been mapped out. Each elementary step in the methanol decomposition reaction into CO and hydrogen occurs via one of three possible mechanisms: O−H, C−H, or C−O bond scission. Multiple reaction pathways for each bond scission have been identified in the present work. Reaction pathway calculations are started from an initial (reactant) state with methanol adsorbed in the most stable geometry on Cu(110). The saddle point and corresponding final state of each reaction or diffusion mechanism were determined without assuming the reaction mechanism. In this way, the reaction paths are determined without chemical intuition. The harmonic pre-exponential factor of each identified reaction is calculated from a normal-mode analysis of the stationary points. Then, using harmonic transition state theory, the rate constant of each identified reaction pathway in the entire reaction network is obtained. The most favorable decomposition route for methanol on Cu(110) is found as follows: $CH_3OH \rightarrow CH_3O \rightarrow CH_2O$. The rate-limiting step in this decomposition route is the dehydrogenation of methoxy to formaldehyde. Our calculations are in agreement with previous experimental observations and theoretical results.

1. Introduction

Understanding complex heterogeneous reactions on catalytic surfaces requires a detailed knowledge of how reaction intermediates interact with the surface and how the bond-breaking and the bond-making processes occur at the active site(s). Finding an accurate description of the spatiotemporal chemical transformation on the catalyst surface under practical reaction conditions is one of the biggest challenges in heterogeneous catalysis. Although state-of-the-art experimental surface science techniques can provide some valuable information on the atomic level, chemical intuition is still needed to propose a reaction mechanism describing the reaction progress and to elucidate experimental observations. In this respect, theoretical studies based upon density functional theory (DFT) calculations have proven useful to complement experimental measurements of reaction products and rates. The mechanism of a heterogeneous catalytic reaction generally consists of a series of elementary steps including the adsorption of reactants, surface reactions (bond-making or bond-breaking), diffusion of surface intermediates, and desorption of products. In order to obtain the thermochemistry and the kinetics of each elementary step from DFT calculations, an initial and final state, and a reaction pathway between them is typically assumed. Then a minimum energy pathway can be optimized locally to identify a transition state along this pathway. An overall reaction path can be obtained from the calculated activation barrier of each elementary step. This approach becomes challenging if there are (as there usually are) different reaction pathways for each elementary step. Calculating one pathway for each elementary step is not necessarily enough to illustrate the complex potential energy surface for reactions on the catalyst surface. Furthermore, the states along an assumed reaction path might not include those

where the bond-breaking or bond-making processes actually occur. Here, we present a methodology that overcomes some of these limitations. Our approach assumes an initial state from which dimer saddle point searches are used to identify (sometimes many) possible reaction mechanisms[1−4] and subsequent intermediate states. Repeating this process, we build a network of states from which the most favorable overall reaction pathway can be determined. We show that this procedure can be used to determine the potential energy surface for the decomposition of methanol on Cu(110) without assuming the reaction mechanism.

Recently, Cu-based catalysts have attracted a great deal of attention for methanol decomposition and synthesis as a possible source of energy for the hydrogen economy.[5,6] Methanol, which is commercially produced from syngas using $Cu/ZnO/Al_2O_3$ catalysts, can be used as the feedstock in direct methanol fuel cells. Steam reforming of methanol on this catalyst has also proven to be an efficient way of producing large quantities of hydrogen. The pioneer experimental work of Wachs and Madix on methanol decomposition on Cu(110) suggested that the clean Cu(110) is not very active for methanol decomposition under UHV condition.[7] Most of the preadsorbed methanol molecules desorb from the surface after heating. Only small amounts of formaldehyde desorb at 370 K.[7,8] X-ray photoelectron spectroscopy (XPS) experiments indicated that methanol decomposes into methoxy on the clean Cu(110) surface at 270 K.[8] Experiments have also shown that two other low-index Cu surfaces, Cu(111)[9] and Cu(100),[10] are inactive to methanol decomposition. With predosed oxygen atoms on the Cu(110) surface, methanol decomposition is significantly facilitated. Besides formaldehyde, other products were observed, such as water which desorbs at 250 K and hydrogen which desorbs at 470 K. Sexton et al. reported similar observations of methanol reactions on Cu(110) using thermal desorption spectroscopy (TDS).[11] The reaction mechanism of methanol decomposition is described as first involving O−H bond scission to form methoxy followed by

* Corresponding author. E-mail: donghai.mei@pnl.gov.
† Pacific Northwest National Laboratory.
‡ University of Texas at Austin.

Methanol Decomposition on Cu(110)

J. Phys. Chem. C, Vol. 113, No. 11, 2009 **4523**

C−H bond scission to form formaldehyde. Since formaldehyde binds weakly on the surface, formaldehyde desorbs from Cu(110) instead of further decomposition to CO and hydrogen (H_2).

Periodic slab DFT calculations have been performed to investigate methanol oxidation on the Cu(110) surface.[12−14] Sakong and Gross found that methanol and formaldehyde are weakly bound to this surface whereas methoxy is strongly bound.[12] In their work, the dissociative adsorption of methanol, yielding surface methoxy and atomic hydrogen, was proposed as the first step in methanol decomposition.[12] The reaction barrier for this step was calculated as 0.73 eV.[12] Recently, these authors reported a similar activation barrier of 0.68 eV for adsorbed methanol dissociation into methoxy.[13] In agreement with experiments, this indicated methanol decomposition is unlikely on the clean Cu(110) surface because the energy for methanol desorption is only 0.34 eV. For the methoxy molecules which do react on the surface, the next step of decomposition leads to formaldehyde and atomic hydrogen with an activation barrier of 1.22 eV.[13] The formate is weakly bound and will rapidly desorb into the gas phase. Comparing the barriers of these two steps, they concluded that the methoxy decomposition is the rate-limiting step in methanol decomposition on Cu(110).[12−14] Greeley and Mavrikakis calculated that methoxy decomposition into formaldehyde is also the rate-limiting step in methanol decomposition on Cu(111).[15]

In this work, we demonstrate a computational methodology based upon DFT and dimer method saddle point searches[1−4] to identify catalytic reaction mechanisms. We use this method to map out the potential energy landscape of complete methanol decomposition on the clean Cu(110) surface. These calculations not only help us to identify other alternative reaction pathways for each elementary steps in the mechanism, which shed light on the complexity nature of methanol decomposition on Cu(110), but also provide a complete picture of the breaking or making of three common bonds (O−H, C−H, and C−O) of all reaction intermediates during methanol decomposition, which might be very useful to other relevant reactions. Furthermore, the calculated potential energy surface can also be used as reference energetic diagram for understanding how the preadsorbed oxygen atoms enhance methanol decomposition on Cu(110).

First, we give a brief description of the computational methodology. Then, starting from the initial state of adsorbed methanol, we identify multiple pathways for each elementary step along the methanol decomposition pathway to obtain a reaction network. Vibrational frequencies are calculated for each state to estimate entropic and quantum effects, and so that the reaction rate constants can be calculated using harmonic transition state theory. The rate-limiting step in methanol decomposition is then determined from our network of rate constants.

2. Computational details

Periodic plane-wave DFT calculations combined with minimum mode following saddle point searches using the dimer method were carried out to explore possible reaction and diffusion pathways in methanol decomposition on the Cu(110) surface. Ion−electron interactions were modeled with the use of ultrasoft pseudopotentials within the framework of the projector augmented wave method.[16,17] The generalized gradient approximation with the Perdew−Wang 91 functional[18] was used to model electron correlation. The geometry of all stationary points were found with the conjugate-gradient algorithm, and

considered converged when the force on each ion dropped below 0.001 eV/Å. The Cu(110)-2×2 surface was modeled with a supercell containing a slab of six atomic layers. Periodic images of the slab were separated by a 10 Å vacuum gap. The bottom four layers were held frozen at equilibrium bulk positions; all other atoms were fully relaxed in our optimizations. Several surface sizes, numbers of atomic layers, and k-point sampling meshes were used to test for convergence. A $2 \times 2 \times 1$ Monkhorst−Pack k-point mesh and a $p(2\times3)$ surface were found to result in relative energies converged to within 0.1 eV. All calculations were performed using the Vienna ab initio simulation package (VASP).[19,20]

Binding energies of adsorbates on the surface, E_b, were calculated as

$$E_b = E_{adsorbate+Cu(110)} - (E_{adsorbate} + E_{Cu(110)}) \quad (1)$$

where $E_{adsorbate+Cu(110)}$ is the energy of the adsorbate molecule interacting with the Cu(110) slab, $E_{Cu(110)}$ is the total energy of bare Cu(110) slab, and $E_{adsorbate}$ is the energy of the gas phase adsorbate molecule.

To find reaction pathways, minimum-mode following searches were used to climb up the potential surface from minima to saddle points. Searches were initiated from stable minima by making a random displacement of the adsorbed molecule(s). From this initial point the dimer method was used to find the lowest curvature mode and follow it to a saddle.[1,3] Each successful search was followed up with a finite-difference normal-mode calculation to verify that a first-order saddle was found and to evaluate the prefactor of the reaction mechanism. The minimum-energy path from each saddle was followed by minimization to determine the initial and final state of the reaction. Additional details of this calculation procedure are included in recent publications.[1−4]

3. Results

3.1. Determination of Initial States. In the present study only the initial state, i.e., the stable methanol adsorption state was used to initiate our exploration of the reaction and diffusion pathways of methanol decomposition. The initial state of each subsequent reaction intermediate is chosen by optimizing the final state of the previous dehydrogenation step, with the coadsorbed atomic hydrogen removed. The reaction intermediates are not required to be in their most stable configurations; they may be kinetic intermediates. The most stable configuration of each surface intermediate is determined by comparing all the configurations identified in our searching processes. Table 1 and Figure 1 list the states of each reaction intermediate used in the exploration of reaction pathways. Other stable adsorption configurations of reaction intermediates that were identified in our search are given in Table 2 and Figure 2.

3.2. Reaction Pathways. *3.2.1. Methanol (CH₃OH) Decomposition.* In the first step, we put one CH_3OH molecule at the top site on Cu(110). As shown in Figure 1a, CH_3OH binds with the uppermost Cu atom through the O atom, which is in agreement with previous experiments.[8] The O−Cu bond is tilted at 18° to the surface normal, and has a length of 2.09 Å, which is slightly shorter than the reported value of 2.16 Å.[13] The calculated binding energy of CH_3OH at the top site is −0.55 eV. This is somewhat weaker than the experimental estimation of −0.70 eV from first-order temperature-programmed desorption (TPD),[7] but stronger than the previous DFT calculation results of −0.41 and −0.34 eV using different functionals.[12,13]
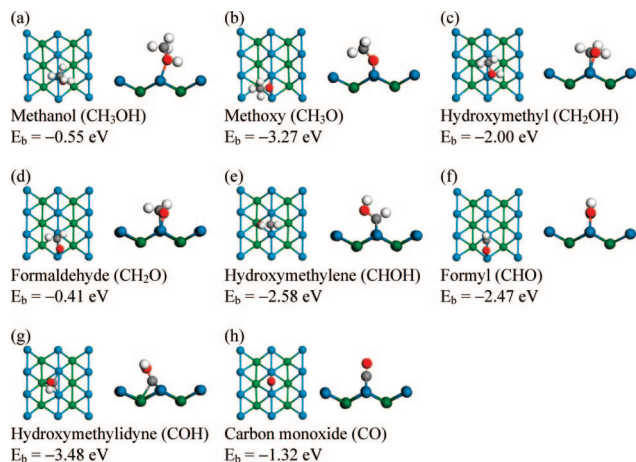
Figure 1. Starting configurations of reaction intermediates used to search for reaction pathways of methanol decomposition on Cu(110). The C, O, and H atoms are gray, red, and white, respectively. The uppermost layer of Cu atoms are blue and the second are green.

3.2.1.1. O−H Scission. The O−H bond scission in CH_3OH yields methoxy (CH_3O) and atomic H. Starting with the adsorbed CH_3OH at the top site, three reaction pathways involving O−H bond scission of CH_3OH have been identified. As shown in Figure 3a, CH_3OH tilts toward the trough in the [001] direction in Path I. As the O−H bond breaks, the CH_3O fragment remains binding at the top site and the dissociated atomic H moves to the short-bridge site on the adjacent Cu row. The distance between the O atom of CH_3O and atomic H is elongated to 1.56 Å. After the transition state, CH_3O and atomic H move further away from each other. The activation barrier of Path I is 0.86 eV, and the reaction energy is +0.33 eV. In the second path, the O−H bond breaks along the [1$\bar{1}$0] direction. CH_3O still stays at the top site while the O−H bond is elongated by moving the hydroxyl H atom to the adjacent pseudo-fcc(111) site. At the final state, CH_3O binds at the short-bridge and atomic H binds at the pseudo-fcc(111) site. The activation barrier for Path II is 1.10 eV. The Path II of O−H bond scission is exothermic, with the reaction energy of −0.19 eV. The third path (Path III) involving O−H bond scission in CH_3OH is similar to the Path II. Instead of binding at the pseudo-fcc(111) site, the atomic H binds at the adjacent short-bridge site at the final state of Path III. The resulting activation barrier is 0.07 eV higher than that of Path II. A fourth path (Path IV) was found in which the CH_3OH first diffuses from the top site to the short-bridge site, at which the binding energy is only 0.05 eV higher than at the top site. From the short-bridge site, the O−H bond breaking of CH_3OH is very similar to the Path I. However, we find that the activation barrier of Path IV is 0.63 eV, which is lower than the barrier of 0.86 eV for Path I. Furthermore, we note that Path IV is exothermic (−0.24 eV) while Path I is endothermic (+0.33 eV). This can be attributed the different configurations of coadsorbed CH_3O in the final states of Path I and IV (top vs the short-bridge site respectively).

Comparing the barriers of the four pathways, it is clear that Path IV is favorable for O−H bond scission of CH_3OH on Cu(110). We also note that the transition states of all four O−H bond scission pathways are "early" transition states in that the configurations of the transition states are close to the initial states. The distance between the O atom of CH_3O and the dissociating H atom is related to the activation barrier; the longer the distance at the transition state, the higher the activation barrier.
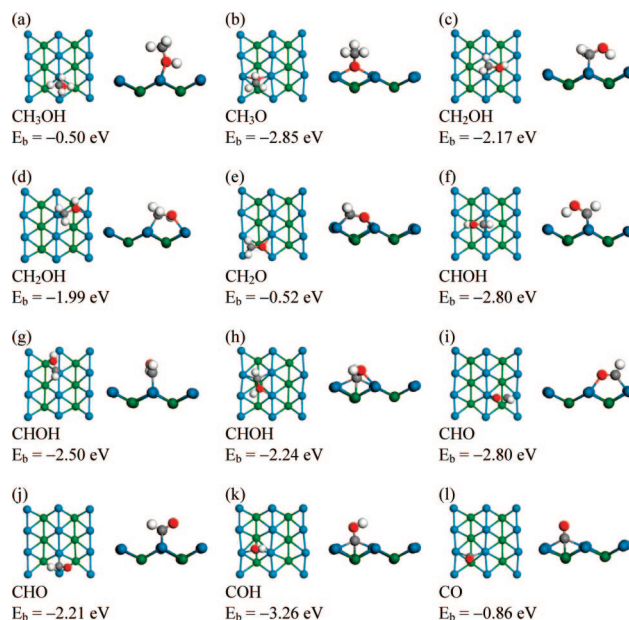

Figure 2. Stable configurations of reaction intermediates identified in the searching process. The color scheme is the same as in Figure 1.

3.2.1.2. C−H Scission. C−H bond scission in CH_3OH produces hydroxymethyl (CH_2OH) and atomic H. Only one such pathway, shown in Figure 3b, was found. The C−H bond in CH_3OH is 1.10 Å at the initial state. The C−H bond scission begins with the rotation of CH_3OH, resulting in hydroxyl group (OH) of CH_3OH moving along the [001] direction to the trough and simultaneously the methyl group (CH_3) moving down to the surface. At the transition state, CH_2OH binds at the top site through the C atom and atomic H binds the adjacent short-bridge site. The broken C−H bond length is 1.87 Å. In the final state, the C-bound CH_2OH moves to the short-bridge site. The distance between the C atom of CH_2OH and the H atom increases to 2.95 Å. The activation barrier for the C−H bond scission of CH_3OH is 1.34 eV. The reaction pathway is endothermic with a reaction energy of +0.74 eV.

3.2.1.3. C−O Scission. Two possible pathways for C−O bond scission of CH_3OH yielding CH_3 and OH have been found. As shown in Figure 3b, OH moves along the [1$\bar{1}$0] direction to the neighboring short-bridge site and CH_3 moves down to the surface as the C−O bond breaks. At the final state of Path I, the O-bound OH binds at the pseudo-fcc(111) site and C-bound CH_3 group binds at the short-bridge site. The activation barrier for Path I is 1.47 eV and the reaction energy is −0.46 eV. The second path of C−O bond scission in CH_3OH (Path II) begins with OH moving toward along the [001] direction to the trough. At the transition state, OH binds at the long-bridge site through the O atom. Then OH continues to move away from CH_3 group. In the final state, the CH_3 group binds at the short-bridge site and OH binds at the short-bridge site on the adjacent Cu row. The barrier of Path II is 1.74 eV, which is higher than Path I.

The first step of CH_3OH decomposition is achieved by breaking one of three bonds (O−H, C−H or C−O). Multiple pathways for each bond scission are identified. In agreement with experimental evidence that only CH_3O was observed on Cu(110),[7,8,11] our results show that the O−H bond scission leading to CH_3O and atomic H is favored.

3.2.2. Methoxy (CH_3O) Decomposition. CH_3O has been well-characterized experimentally as a reaction intermediate in methanol decomposition on the Cu(110) surface.[7,8,11] Ultraviolet photoelectron spectroscopy (UPS) experiments show that CH_3O

TABLE 1: Geometric and Energetic Parameters of Reaction Intermediates Used To Search for Possible Reaction Pathways

reaction intermediates	configuration	bond lengths (Å)	binding energy (E_b)	
			without ZPEC	with ZPEC
CH_3OH	top, O-bound	$d(O-Cu) = 2.09$	-0.55	-0.45
CH_3O	short-bridge, O-bound	$d(O-Cu) = 1.97$	-3.27	-3.16
CH_2OH	short-bridge, C-bound and O-bound	$d(O-Cu) = 2.10$	-2.00	-2.00
		$d(C-Cu) = 1.98$		
CH_2O	short-bridge, C-bound and O-bound	$d(O-Cu) = 2.05$	-0.41	-0.38
		$d(C-Cu) = 2.21$		
$CHOH$	short-bridge, C-bound	$d(C-Cu) = 1.99$	-2.58	-2.52
CHO	short-bridge, C-bound and O-bound	$d(O-Cu) = 2.02$	-2.47	-2.46
		$d(C-Cu) = 1.92$		
COH	pseudo-fcc(111), C-bound	$d(C-Cu) = 2.11$	-3.48	-3.35
		$d(C-Cu) = 1.91$		
CO	short-bridge, C-bound	$d(C-Cu) = 1.97$	-1.32	-1.31

TABLE 2: Geometric and Energetic Parameters of Reaction Intermediates as Identified Stable States

reaction intermediates	configuration	bond lengths (Å)	binding energy (E_b) without ZPEC
CH_3OH	short-bridge, O-bound	$d(O-Cu) = 2.21$	-0.50
		$d(O-Cu) = 2.46$	
CH_3O	long-bridge, O-bound	$d(O-Cu) = 2.07$	-2.85
CH_2OH	short-bridge, C-bound	$d(C-Cu) = 2.10$	-2.17
	long-bridge, C-bound and O-bound	$d(O-Cu) = 2.04$	-1.99
		$d(C-Cu) = 2.19$	
CH_2O	long-bridge, C-bound and O-bound	$d(O-Cu) = 2.05$	-0.52
		$d(C-Cu) = 2.21$	
$CHOH$	short-bridge, C-bound	$d(C-Cu) = 2.00$	-2.80
	top, C-bound	$d(C-Cu) = 2.00$	-2.50
	long-bridge, C-bound and O-bound	$d(O-Cu) = 2.18$	-2.24
		$d(C-Cu) = 2.04$	
CHO	long-bridge, C-bound and O-bound	$d(C-Cu) = 2.17$	-2.80
		$d(O-Cu) = 2.01$	
	short-bridge, C-bound	$d(C-Cu) = 1.92$	-2.21
		$d(C-Cu) = 2.07$	
COH	long-bridge, C-bound	$d(C-Cu) = 1.98$	-3.26
CO	long-bridge, C-bound	$d(C-Cu) = 2.09$	-0.86

adsorbs on Cu(110) through the O atom with an off-normal orientation.[8,11] In agreement with experiments, our calculation show that CH_3O binds at the short-bridge site through the O atom. As shown in Figure 1b, the C−O axis of CH_3O tilts in the [001] and the [1$\bar{1}$0] direction by 13° and 33°, respectively. This is not quite consistent with previous Near Edge X-ray Absorption Fine Structure (NEXAFS) result that the C−O axis is tilted by 36° ± 5° in both azimuths.[21] The binding energy of CH_3O at the short-bridge site is −3.27 eV, slightly stronger than previously reported DFT value of −2.98 eV.[13] The O−Cu bond length of adsorbed CH_3O at the short-bridge site is 1.97 Å, in good agreement with the result of 1.96 Å.[13] The possible reaction pathways for CH_3O decomposition are either via C−H bond scission or C−O bond scission. The initial state used for searching is CH_3O binding at the short-bridge site.

3.2.2.1. C−H Scission. Breaking the C−H bond in CH_3O leads to formaldehyde (CH_2O) and atomic H. When the C−H bond breaks, one of methylic H atom of CH_3 moves to the adjacent short-bridge site in the [1$\bar{1}$0] direction. The C−H distance elongates from 1.11 Å at the initial state to 1.73 Å at the transition state. The activation barrier of the C−H bond scission in CH_3O is 1.11 eV. The reaction energy is +1.01 eV, indicating this reaction pathway is highly endothermic. This also implies that the reverse pathway that CH_2O recombines with atomic H to forming CH_3O readily occurs. We also calculated the binding energies of atomic H on the Cu(110) surface. The binding energies of atomic H at the short-bridge and the pseudo-fcc(111) site are −2.41 and −2.35 eV. Considering that the binding energy of CH_2O at the short-bridge site is only −0.41

eV, a strong repulsive interaction of 0.56 eV between coadsorbed bridging CH_2O and atomic H at the final state is found. Therefore, it is expected that the atomic H will quickly diffuse from the short-bridge site to the neighboring pseudo-fcc(111) site. Sakong and Gross reported a reaction pathway for the decomposition of CH_3O via C−H bond scission to produce CH_2O in the gas phase and surface atomic H on the surface with an activation barrier between 1.22[13] and 1.44 eV.[12,14] Furthermore, there is only a small barrier (0.2 eV) for CH_3O formation via gas-phase CH_2O directly reacting with adsorbed H atom.[12−14] Our calculations are consistent with the result of Sakong and Gross.[12] Methoxy decomposition into formaldehyde by either reaction pathway is comparable due to the weak interaction between CH_2O and Cu(110).

3.2.2.2. C−O Scission. CH_3O decomposition via C−O bond scission yields CH_3 and atomic O. As shown in Figure 4, two reaction pathways (I and II) for C−O bond scission in CH_3O are found. The difference between these two pathways is the moving direction of CH_3 as the C−O bond ruptures. CH_3 moves along the [1$\bar{1}$0] direction in Path I while moves along the [001] direction in Path II. We note that CH_3 still binds at the top site through the C−Cu bond in Path I at the transition state, while CH_3 has been lifted off the surface in Path II. At the final state, CH_3 binds at the short-bridge site and atomic O binds at the adjacent pseudo-fcc(111) site. Both Paths I and II are endothermic with the reaction energies of +0.32 and +0.26 eV. The activation barriers of C−O bond scission in Paths I and II are 1.67 and 2.10 eV, respectively, indicating that C−O bond
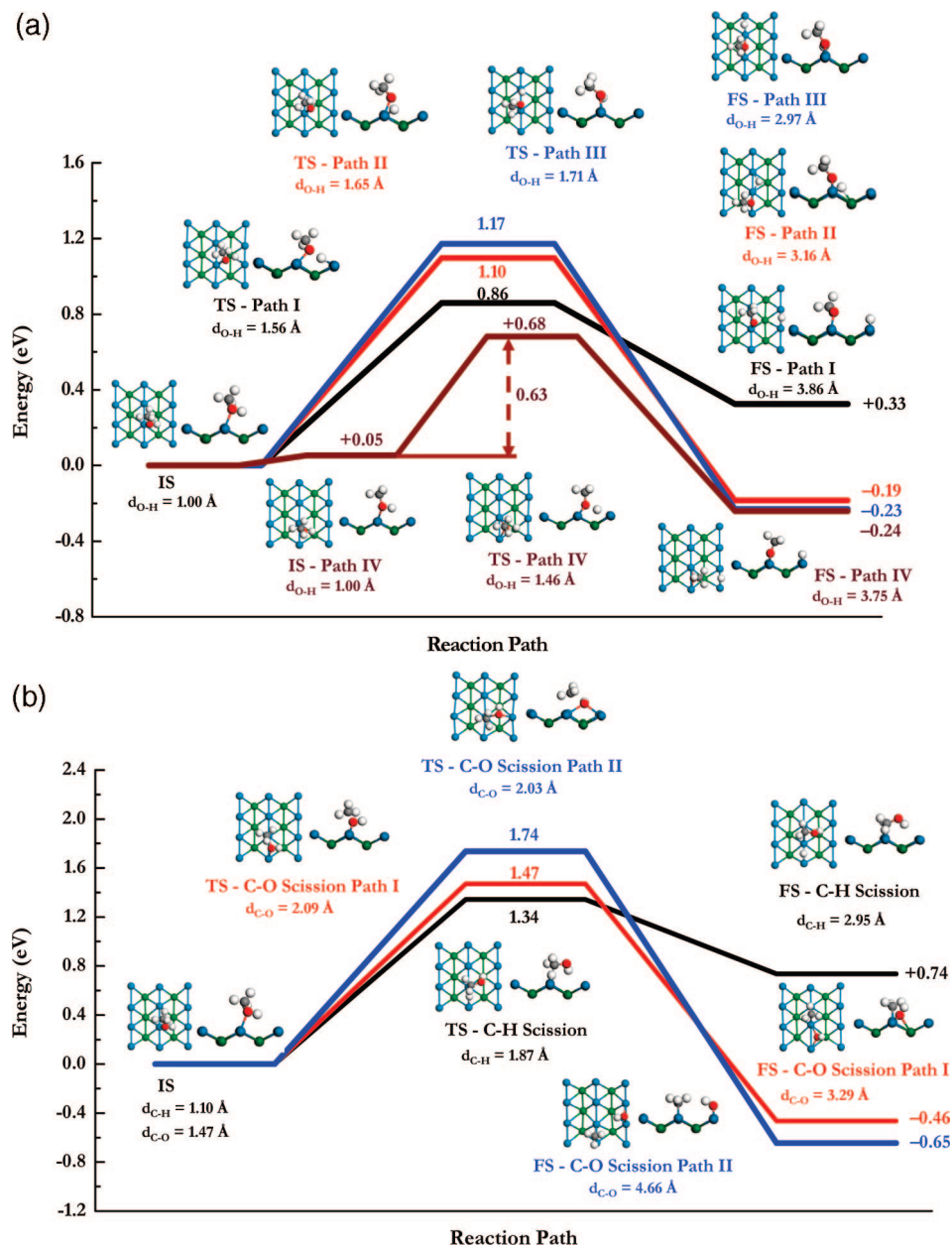
Figure 3. Reaction pathways of CH$_3$OH: (a) O−H scission; (b) C−H and C−O scission. IS: Initial State; TS: Transition State; FS: Final State.

scission of CH$_3$O is unlikely. C−H bond scission of CH$_3$O yielding CH$_2$O is the possible pathway for CH$_3$O decomposition.

3.2.3. Hydroxymethyl (CH$_2$OH) Decomposition. CH$_2$OH is considered an important reaction intermediate in methanol decomposition on Pt(111) because of the competitive paths of O−H and C−H bond scission of CH$_3$OH on Pt(111),[22−24] although it is not observed experimentally on Pt(111). As we discussed in section 3.2.1, the O−H bond scission of CH$_3$OH yielding CH$_3$O is significantly more favorable than the C−H bond scission of CH$_3$OH yielding CH$_2$OH. In order to completely explore the reaction network of CH$_3$OH decomposition on Cu(110), we study the decomposition of CH$_2$OH because CH$_2$OH might be connected with other reaction intermediates in CH$_3$OH decomposition.

To the best of our knowledge, no theoretical study of CH$_2$OH adsorption and decomposition on Cu(110) has been reported. One DFT calculation suggested that CH$_2$OH adsorbed at the top site through the C atom on Cu(111).[25] In the present work, three adsorption configurations for CH$_2$OH on Cu(110) are

found. Among them CH$_2$OH adsorbed at the short-bridge site through the C atom (Figure 2c) is found to be the most stable configuration. The binding energy of CH$_2$OH at the short-bridge site is −2.17 eV. CH$_2$OH also binds at the short-bridge site with both C−Cu and O−Cu bonding (Figure 1c). This double bonding configuration of CH$_2$OH at the short-bridge is slightly weaker (by 0.17 eV) than the single C−Cu bonding configuration. The third configuration is that CH$_2$OH binds at the long-bridge site (Figure 2d). The binding energy of CH$_2$OH at the long-bridge site is −1.99 eV, which is the same as that at the short-bridge site with double bonds. For CH$_2$OH decomposition, three bond scissions (O−H, C−H, and C−O) of CH$_2$OH are possible. The adsorbed CH$_2$OH at the short-bridge site with double bonds is used as the initial state for searching possible reaction paths.

3.2.3.1. O−H Scission. The O−H bond scission of CH$_2$OH yields CH$_2$O and the atomic H. Four identified reaction pathways for O−H bond scission are shown in Figure 5a and 5b. In Path I, as the O−H bond breaks, hydroxyl H moves along the [001]
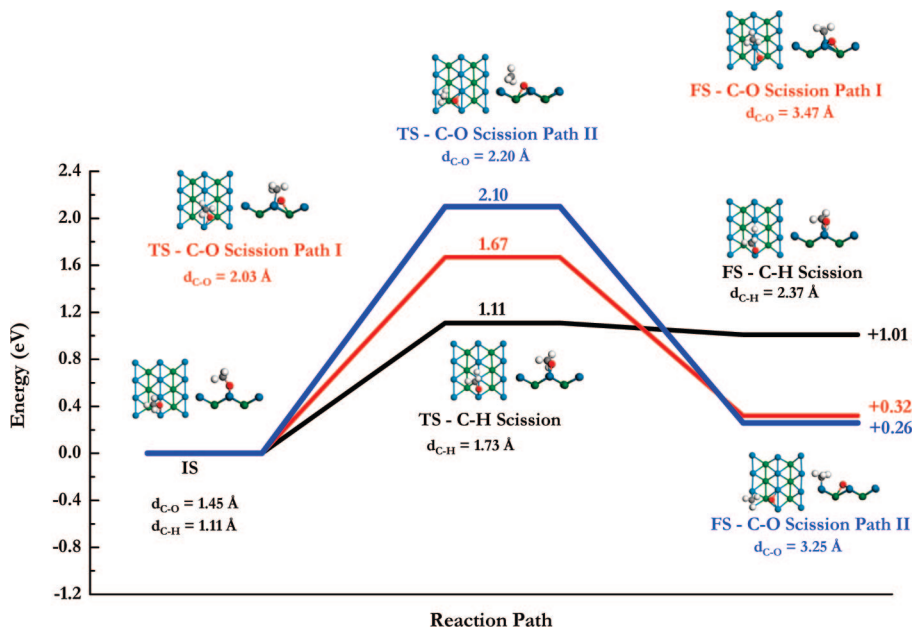
Figure 4. Reaction pathways of CH₃O.
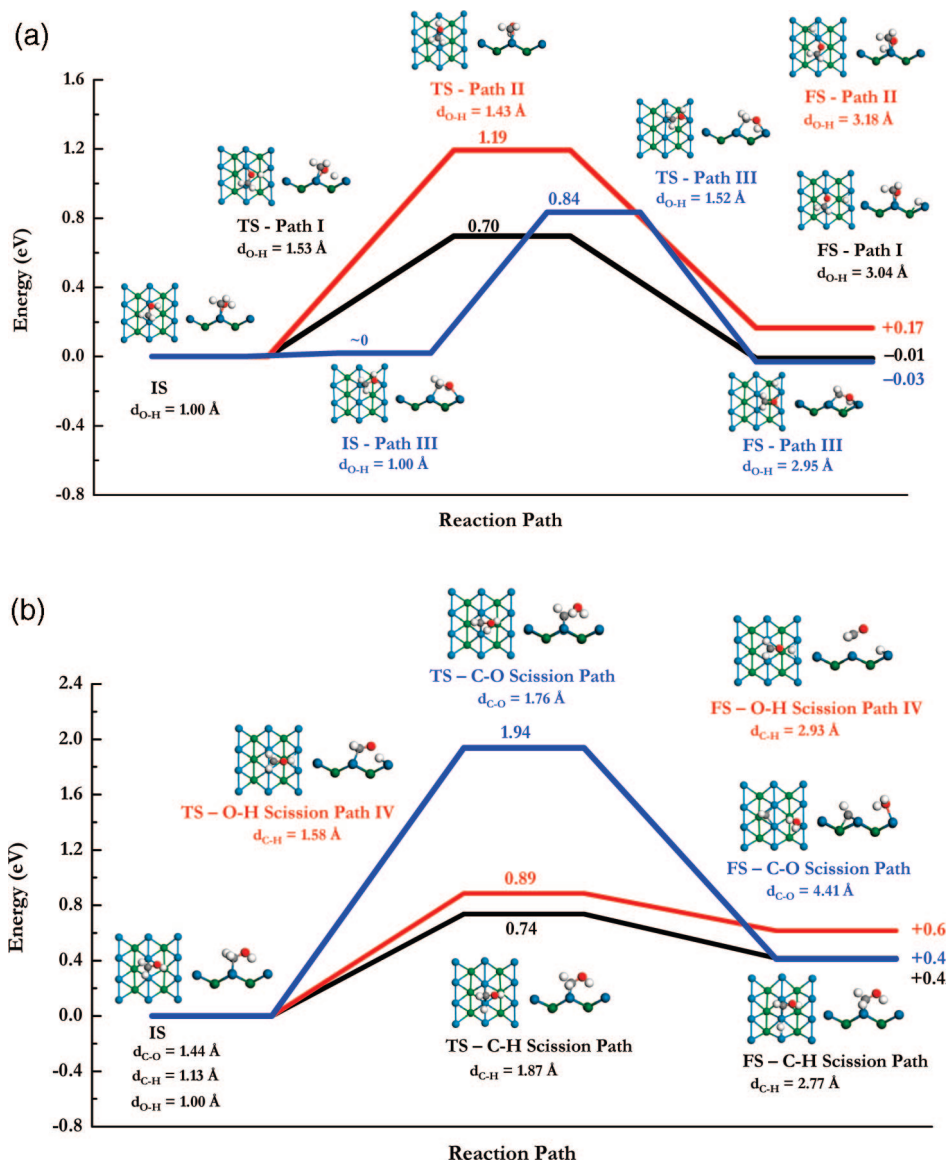
Figure 5. Reaction pathways of CH₂OH: (a) O−H scission; (b) O−H, C−H, and concurrent C−H and C−O scission.

direction while the CH_2O fragment remains at the short-bridge site. The distance between the O atom of the CH_2O fragment and the hydroxyl H elongates to 1.53 Å at the transition state. The activation barrier of O−H bond scission of CH_2OH in Path I is 0.70 eV. Path I is thermochemically neutral. In Path II, the O−H bond breaks along the $[1\bar{1}0]$ direction. The activation barrier of Path II is 1.19 eV. Path II is slightly endothermic with the reaction energy of +0.17 eV. In Path III, adsorbed CH_2OH migrates from the short-bridge site to the long-bridge site before the O−H bond breaks. Then the O−H bond breaks along the $[1\bar{1}0]$ direction, yielding the coadsorbed CH_2O at the long-bridge site and atomic H at the pseudo-fcc(111) site. The activation barrier of Path III is 0.84 eV. Like Path I, Path III is thermochemically neutral. Path IV of O−H bond scission of CH_2OH is shown in Figure 5b (labeled Path IV). Path IV is a reaction pathway that the dissociated CH_2O will be released to the gas phase after O−H bond scission. At the initial state of Path IV, CH_2OH binds at the short-bridge site only through the C atom. The activation barrier of Path IV is 0.89 eV. The reaction energy of Path IV is +0.62 eV. The high endothermicity of Path IV indicates that the reverse process that adsorption of formaldehyde with the preadsorbed atomic H forming CH_2OH is very likely occurring on Cu(110).

3.2.3.2. C−H Scission. The C−H bond scission of CH_2OH produces hydroxymethylene (CHOH) and atomic H. Only one pathway for C−H bond scission is identified. As shown in Figure 5b, this C−H scission pathway starts with the C-bonded CH_2OH at the short bridge. As the C−H bond breaks, the methylic H moves away from CHOH along the $[1\bar{1}0]$ direction. The activation barrier of C−H scission in CH_2OH is 0.74 eV. The reaction energy is +0.42 eV.

3.2.3.3. Concurrent C−O and C−H Scissions. The reaction pathway for C−O bond scission in CH_2OH to yield methylene (CH_2) and OH is not identified in the present work. Instead, we identify an alternative pathway that CH_2OH dissociates into methylidyne (CH) and water (H_2O) via both C−O and C−H bond scissions. When the C−O bond of CH_2OH is breaking, one of the C−H bonds in CH_2OH is also broken. The methylic H then recombines with the dissociated OH group forming H_2O. At the final state, CH binds at the pseudo-fcc(111) site and H_2O binds at the top site with a slightly tilted orientation. Since this special reaction pathway involves two bond-breaking processes and one bond-making process, the activation barrier is very high (1.94 eV). The calculated reaction energy is +0.41 eV.

Comparing the activation barriers of the reaction pathways found for CH_2OH dissociation on Cu(110), we find that the O−H scission (Path I) and the C−H scission are competitive due to their similar barriers (0.70 vs 0.74 eV). This suggests that both CH_2O and CHOH species can be formed via CH_2OH decomposition. A reaction pathway, which releases CH_2O into the gas phase, is also possible with a somewhat higher barrier of 0.89 eV, providing an alternate route for CH_2OH formation from CH_2O. The direct formation via C−H bond scission of CH_3OH is unlikely.

3.2.4. Formaldehyde (CH_2O) Decomposition. CH_2O is the only experimentally observed product in CH_3OH TPD on the clean Cu(110) surface. We find CH_2O weakly binds at the short-bridge site through both C and O atoms. As shown in Figure 1d, the axis of adsorbed CH_2O is slightly tilted away from the $[1\bar{1}0]$ direction. The C−Cu and O−Cu bond lengths are 2.21 and 2.05 Å, respectively. The binding energy of CH_2O at the short-bridge site is −0.41 eV. This is in good agreement with previous DFT result of 0.46 eV.[13] CH_2O also binds at the long-bridge site on Cu(110). The binding energy of CH_2O at the long-

bridge site is −0.52 eV. Our calculated binding energies of CH_2O are slightly weaker than the experimental result of 0.59 eV.[11] For CH_2O decomposition, only two bond scissions (C−H and C−O) are possible. Unfortunately, there are no theoretical calculations of CH_2O decomposition on Cu(110) that we can compare with. The adsorbed CH_2O at the short-bridge site is used as the initial state.

3.2.4.1. C−H Scission. The C−H bond scission of CH_2O yields formyl (CHO) and atomic H. Starting with adsorbed CH_2O at the short-bridge site, three possible reaction paths for the C−H bond breaking are found. As shown in Figure 6a, all three paths are endothermic, indicating the reverse process that recombines CHO and atomic H forming CH_2O is more favorable. Path I shows the C−H bond breaks along the [001] direction. The coadsorbed CHO and atomic H bind at the short-bridge sites on separate uppermost rows in the final state of Path I. The activation barrier of Path I is 0.79 eV. In Path II, the C−H bond breaks along the $[1\bar{1}0]$ direction. The activation barrier for Path II is 0.95 eV. Similar to the bond-breaking processes discussed above, this implies the C−H bond breaking of CH_2O along the [001] direction is preferred to that along $[1\bar{1}0]$. The lowest energy mechanism, path III, consists of two steps. CH_2O first diffuses from the short-bridge site to the long-bridge site with a barrier is 0.47 eV. Then CH_2O dissociates into CHO and atomic H with an activation barrier of 0.68 eV. In the final state, CHO binds at the long-bridge site and atomic H binds at the short-bridge site.

3.2.4.2. C−O Scission. The C−O bond scission of CH_2O yields CH_2 and atomic O. Figure 6b shows two such reaction pathways, both of which involve significant surface relaxation. At the transition state of Path I, atomic O binds at the pseudo-fcc(111) site while CH_2 binds at the pseudo-bridge site. At the final state, CH_2 binds at the short-bridge site and atomic O binds at the adjacent pseudo-fcc(111) site. The activation barrier of Path I is 1.28 eV. Path I is endothermic with the reaction energy of +0.51 eV. Path II is similar to the Path III of C−H bond scission of CH_2O. CH_2O diffuses from the short-bridge site to the long-bridge site; the C−O bond is broken; and in the final state, CH_2 binds at the long-bridge site and the atomic O binds the pseudo-fcc(111) site. The activation barrier of Path II is very high (1.82 eV). In conclusion, the most favorable dissociation path for CH_2O is via C−H bond scission leading to CHO and atomic H, i.e., the Path III in Figure 6a.

3.2.5. Hydroxymethylene (CHOH) Decomposition. Experimental information of CHOH interacting with metal surfaces has not been reported before. However, it is important to keep in mind that many reaction intermediates cannot be observed by spectroscopic techniques because they are highly reactive and have short lifetimes on the surface. A DFT study suggested that CHOH adsorbs at the 3-fold hollow site on Cu(111) through the C atom.[25] Other slab DFT calculation indicated that CHOH adsorbs on the bridge site on Pt(111).[24] Our calculations show that CHOH prefers to bind at the short-bridge site on Cu(110) through the C atom. At the short-bridge site, two orientations of the CHOH hydroxyl have been identified. The hydroxyl H atom can either point away from the surface (Figure 1e) or toward the surface (Figures 2f). As expected, the configuration with hydroxyl H atom pointing to the surface is slightly more stable (by 0.21 eV). The rotation barrier between these states is 0.26 eV. Besides the short-bridge site, CHOH can also bind at the top site (Figures 2g) and the long-bridge site (Figure 2h) with the binding energies of −2.50 and −2.24 eV.

3.2.5.1. O−H Scission. The O−H bond scission of CHOH yields CHO and atomic H. Three O−H bond scission pathways
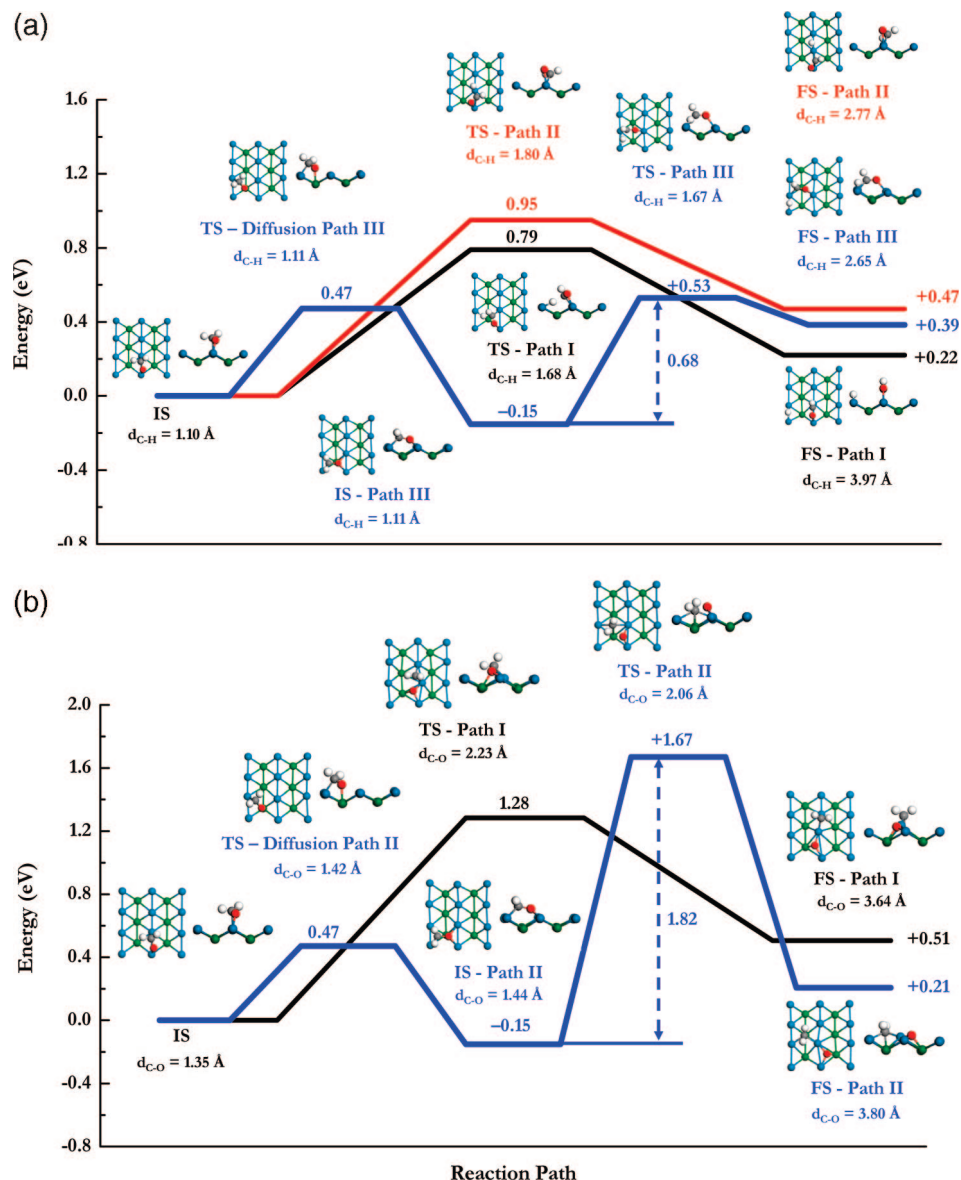
Figure 6. Reaction pathways of CH_2O: (a) $C-H$ scission; (b) $C-O$ scission.

with different initial states for CHOH have been identified in this work. The most favorable path is Path I (see Figure 7a), in which CHOH at the short-bridge site dissociates into CHO at the short-bridge site and atomic H at the pseudo-fcc(111) site. The activation barrier of Path I is 0.70 eV, and the reaction energy is +0.29 eV. The Path II of O—H scission begins with the adsorbed CHOH at the top site. The initial state in Path II is 0.26 eV less stable than the initial state in Path I. The O—H bond breaks along the [1$\bar{1}$0] direction. At the final state, CHO binds at the short-bridge site through the C atom and atomic H binds at the adjacent pseudo-fcc(111) site. The activation barrier of Path II is 1.18 eV and the reaction pathway is endothermic with the reaction energy of +0.60 eV. The Path III of O—H bond scission of CHOH begins with the initial state that CHOH binds at the long-bridge site. Although the activation barrier for Path III is 0.59 eV, smaller than the barrier of Path I, the initial state of Path III is 0.56 eV less stable than the corresponding initial state of Path I. As a result, the total barrier of Path III is at least 1.15 eV. Therefore, Path I is the favorable pathway for O—H scission of CHOH.

3.2.5.2. C—H Scission. The second possible CHOH decomposition path is via C—H bond scission, producing hydroxym-

ethylidyne (COH) and atomic H. Three pathways (all endo-thermic) are shown in Figure 7b. In Path I, the C-bonded CHOH at the short-bridge moves to the trough along the [001]direction as the C—H bond breaks. In the final state, both COH and atomic H bind at adjacent pseudo-fcc(111) sites. The C—H bond-breaking barrier of Path I is 1.02 eV. In Path II, COH and atomic H move in the opposite direction, dissociating with an activation barrier of 1.14 eV. Path II is highly endothermic so that the dissociated COH and H will quickly recombine to form CHOH. In the third path, the hydroxyl H initially rotates from an upward direction to a downward direction (pointing at the surface) before the C—H bond breaks. In the final state, COH binds at the pseudo-fcc(111) site while atomic H binds at the short-bridge site. The activation barrier for Path III is 1.36 eV, which is higher than the barriers of paths I and II.

3.2.5.3. C—O Scission. Three pathways for C—O bond scission of CHOH were identified (see Figure 7c), each yielding methylidyne (CH) and OH. In Path I, CHOH moves to the trough along the [001]direction. At the transition state, both CH and OH bind at the pseudo-fcc(111) sites. Then OH group continues to move along the [001]direction and finally binds at the short-bridge site on the cross row while CH remains at the
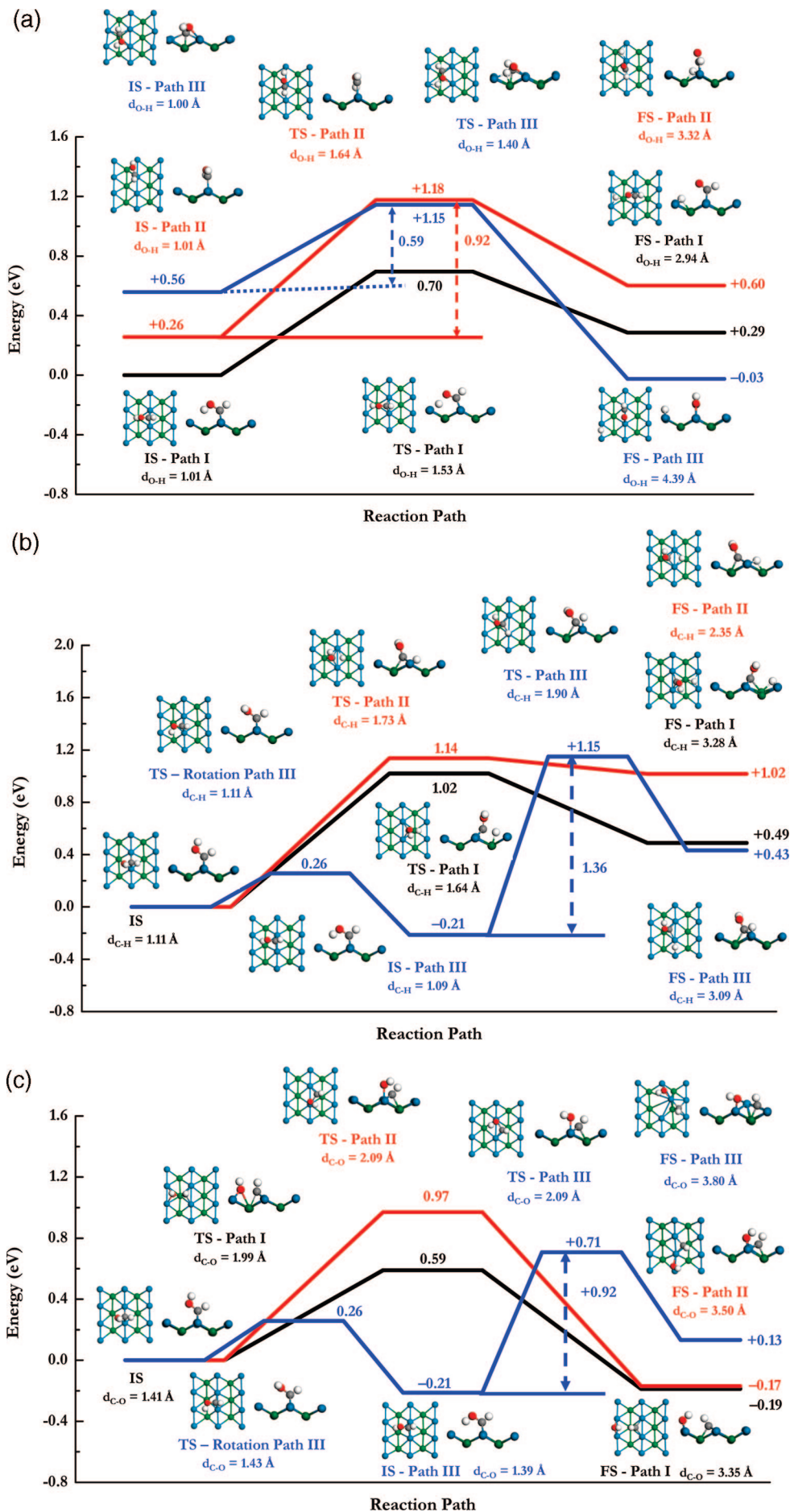
Figure 7. Reaction pathways of CHOH: (a) O−H scission; (b) C−H scission; (c) C−O scission.
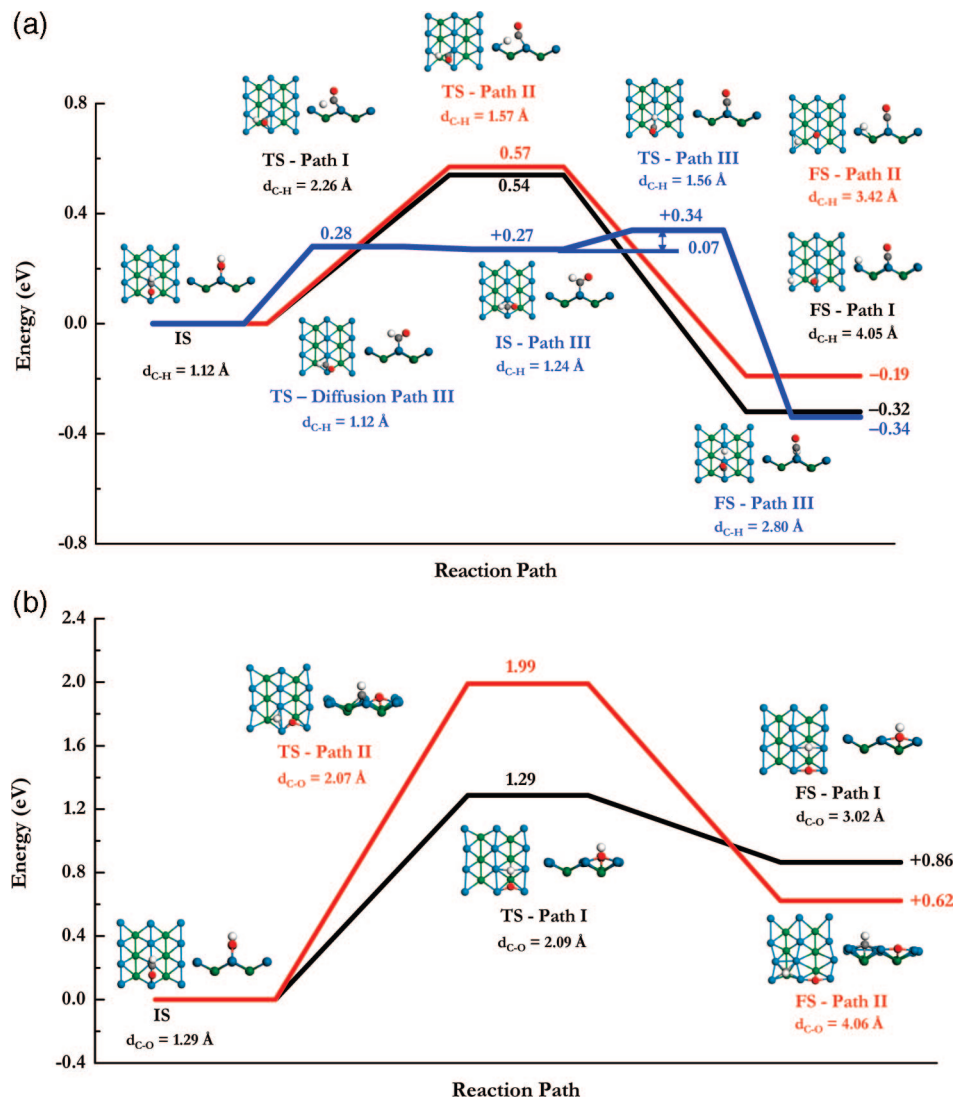
Figure 8. Reaction pathways of CHO: (a) C–H scission; (b) C–O scission.

original pseudo-fcc(111) site. The activation barrier of Path I is 0.59 eV. In Path II, instead of moving along the [001] direction, CHOH moves along the [1$\bar{1}$0] direction as the C–O bond breaks. The final state is the coadsorbed CH binding at the pseudo-fcc(111) site and OH binding at the short-bridge site through the O atom. Although the reaction energies of Path I and II are close (−0.19 and −0.17 eV), the activation barrier of Path II is higher (0.97 eV). Path III goes through an H rotation process before the C–O bond breaking. We note that a significant surface relaxation is observed in Path III. One of uppermost Cu atoms on the surface is lifted off and moved right over the trough. This can be attributed to the strong interaction between CH and Cu(110). A complex of CH–Cu–OH configuration is formed at the final state of Path III. The activation barrier of Path III is 0.92 eV and is endothermic by +0.34 eV. Comparing all reaction pathways found for CHOH decomposition, Path I of C–O bond scission is slightly preferred, but might be competitive with Path I of O–H bond scission. This indicates that both CH and CHO are the possible products by CHOH decomposition on Cu(110).

3.2.6. Formyl (CHO) Decomposition. As far as we know, no direct experimental spectroscopic signature of CHO had ever been reported in methanol decomposition on transition-metal surfaces. This is due to the fact that CHO is a radical species which is highly reactive on the surface.[15] Theoretical investiga-

tions have been performed to provide energetic and structural information of CHO adsorption on metal surfaces. Previous cluster and slab DFT calculations suggested that CHO binds at 3-fold hollow site on Cu(111) through the C atom.[15,25,26] We identify three stable adsorption positions for CHO on Cu(110) in the present work. The most stable configuration which is shown in Figure 2i has CHO adsorbed at the long-bridge site through both the C and O atoms with a binding energy of −2.80 eV. CHO can also bind at the short-bridge site with both C and O atoms (Figure 1f) or through the C atom only (Figure 2j), binding with −2.47 and −2.21 eV, respectively. There are no DFT calculations of CHO adsorption on Cu(110) reported that we can compare with. The reported binding energies of CHO on Cu(111) are in the range of 1.15−1.45 eV;[15,25,26] therefore, it is clear that the adsorption of CHO on Cu(110) is much stronger. The adsorbed CHO at the short-bridge site with both C–Cu and O–Cu bonds is chosen as the initial state to explore its decomposition pathways. Two bond scissions (C–O and C–H) of CHO are possible for CHO decomposition.

3.2.6.1. C–H Scission. First, we discuss the pathways for the C–H scission of CHO. As shown in Figure 8a, CHO dissociates into CO and atomic H via C–H bond scission by three different pathways. In Path I, CO binds at the short-bridge site and atomic H binds at the short-bridge site on the cross row at the final state; while CO binds at the top site and atomic

H binds at the pseudo-fcc(111) site in Path II. The activation barriers for Path I and II are very close; 0.54 eV for Path I and 0.57 eV for Path II, and are exothermic with reaction energies of −0.32 and −0.19 eV, respectively. In the third path, CHO rotates from the [1$\bar{1}$0] to the [001] direction and, as a result, switches from double C−Cu and O−Cu bonding to single C−Cu bonding at the short-bridge site. The diffusion barrier for this rotation process is 0.28 eV. We note that CHO adsorbed at the short-bridge site through single C−Cu bonding is unstable since there is a negligible reverse barrier. Therefore, the single C−Cu bond at the short-bridge site can also be considered an intermediate state in the C−H bond scission. From this intermediate state, the C−H bond scission of CHO in Path III is nearly spontaneous with an activation barrier of only 0.07 eV. The total activation barrier for C−H bond scission in Path III is 0.35 eV, making it the most favorable.

3.2.6.2. C−O Scission. The C−O bond scission of CHO yields CH and atomic O. Figure 8b shows two identified reaction pathways for C−O bond scission of CHO. In Path I, the short-bridge bonded CHO moves to the trough along the [001] direction as the C−O bond breaks. At the transition state, both CH and atomic O binds at the long-bridge sites with the C−O distance of 2.09 Å. The activation barrier for Path I is 1.29 eV and the reaction is endothermic (+0.86 eV). Path I is a product-like reaction pathway because the geometrical configurations of the transition state and the final state are similar. In Path II, the atomic O moves to the long-bridge site while the CH group moves to adjacent pseudo-fcc(111) site in the opposite direction when the C−O bond breaks. As shown in Figure 8b, a pronounced surface relaxation of Cu(110) is observed in Path II. At the final state, both CH and atomic O bind at the long-bridge sites sharing one uppermost Cu atom. It is generally observed from the calculations of this work that the significant surface relaxation (reconstruction) occurs when the products involving unsaturated hydrocarbon species (CH$_x$). Path II is endothermic with the reaction energy of +0.62 eV. The activation barrier of in Path II is very high (1.99 eV) so that the process is unlikely. Compared with the calculated activation barriers of different pathways for both C−H and C−O bond scissions of CHO, the C−H bond scission of CHO leading to CO and atomic H is the dominated pathway for CHO decomposition on Cu(110).

3.2.7. Hydroxymethylidyne (COH) Decomposition. COH species is the product of HCOH decomposition via C−H bond scission. Previous cluster and periodic DFT studies of COH on Pt(111) and Cu(111) suggest that COH binds at a 3-fold hollow site through the C atom.[25] In agreement with these theoretical results, the most stable adsorption site for COH on Cu(110) is the pseudo-fcc(111) site. As shown in Figure 1g, the C−O axis of adsorbed COH is tilted by 35° with respect to the surface normal. The angle of C−O−H is 111°. The three C−Cu bond lengths are 2.11, 1.91, and 1.91 Å. The binding energy of adsorbed COH at the pseudo-fcc(111) site is −3.48 eV, indicating that COH binds on Cu(110) stronger than on Cu(111) with the binding energy of −2.95 eV.[25] COH can also bind upright at the long-bridge site with two C−Cu bonds (Figure 2k). The binding energy of COH at the long-bridge is −3.24 eV, slightly weaker than the pseudo-fcc(111) site. The diffusion barrier for COH moving from the pseudo-fcc(111) site to the long-bridge site is 0.34 eV. We find that COH stays at pseudo-bridge site at the transition state in the diffusion. The barrier for the reverse diffusion path is only 0.11 eV, indicating that COH prefers to stay at the most stable pseudo-fcc(111) site. The pseudo-fcc(111) site is used as the initial state for searching

the possible reaction pathways of COH decomposition. The O−H and C−O bond scissions of COH are possible for COH decomposition.

3.2.7.1. O−H Scission. The O−H bond scission of COH produces CO and atomic H. Two reaction pathways of O−H scission shown in Figure 9a are found. In Path I, the O−H bond scission begins with the rotation of hydroxyl H atom of COH from the [1$\bar{1}$0] direction to the [001] direction. At the transition state, the O−H bond is already broken since the distance between O and H is 1.23 Å. After the transition state, atomic H continues to move away from CO and finally binds at the short-bridge site while CO also moves from the pseudo-fcc(111) site to the short-bridge site with an upright orientation at the final state. The activation barrier of Path I is 0.34 eV, and the reaction energy is −1.06 eV, highly exothermic. In Path II, the O−H bond breaking starts with the H atom of COH moving to the adjacent short-bridge site along the [1$\bar{1}$0] direction. At the final state, both atomic H and CO bind at the adjacent short-bridge sites. Although the reaction energies of Path I and II are nearly the same, the activation barrier of Path II is higher (0.91 eV), indicating that Path I is the preferred reaction pathway for the O−H bond. The activation barrier of COH dehydrogenation to CO and H was calculated as 1.05 eV on Cu(111).[25] The O−H scission path of COH on Cu(111) is also highly exothermic (−1.19 eV).[25]

3.2.7.2. C−O Scission. The C−O bond scission of COH yields carbon (C) and OH. Three possible C−O bond scission pathways have been identified. Path I and Path II begin with the most stable pseudo-fcc(111) site. In Path III, COH migrates to the long-bridge site where the bond-breaking occurs. As mentioned previously, we attribute the significant surface relaxation of Cu(110) induced by the formation of the unsaturated hydrocarbon species to the strong interaction between C and the Cu(110) surface. A pronounced surface relaxation observed in the final states of Path I and II further confirms this. As shown in Figure 9b, after the C−O bond breaking, the C atom at the pseudo-fcc(111) site further moves inward to the Cu(110) surface, yielding two bonded Cu atoms, one in the uppermost row and another in the second row, that migrate away from their original equilibrium positions. As a result, the pseudo-fcc(111) site becomes the pseudo-4-fold hollow site. A similar trend that the barrier for the bond-breaking process along the [001] direction is lower than that along the [1$\bar{1}$0] direction on Cu(110) is found again. The C−O scission along the [001] direction has a lower activation barrier. The activation barrier for Path I is 1.14 eV, which is lower than the barrier of 1.59 eV in Path II. Path III starts with adsorbed COH on the long-bridge site. As the C−O bond breaks, the C atom still stays at the long-bridge site and the OH group moves to the bridge fcc(111) site at the transition state. OH group binds at the short-bridge site in the final state. However, we note that little surface relaxation is found in Path III. The activation barrier of Path III is 0.81 eV, which is lower than the barriers of Path I and II, indicating that Path III is the most favorable path for the C−O bond scission of COH. Interestingly, although the barriers of three C−O scission pathways of COH are quite different, all three reaction pathways are nearly thermochemically neutral. The reaction energies of three paths are +0.14, −0.15, and +0.16 eV, respectively.

Because the lowest activation barrier pathway of C−O bond scission in COH is still much higher than the barrier for O−H scission pathways, it is expected that COH decomposition proceeds via O−H bond scission, yielding CO and atomic H.
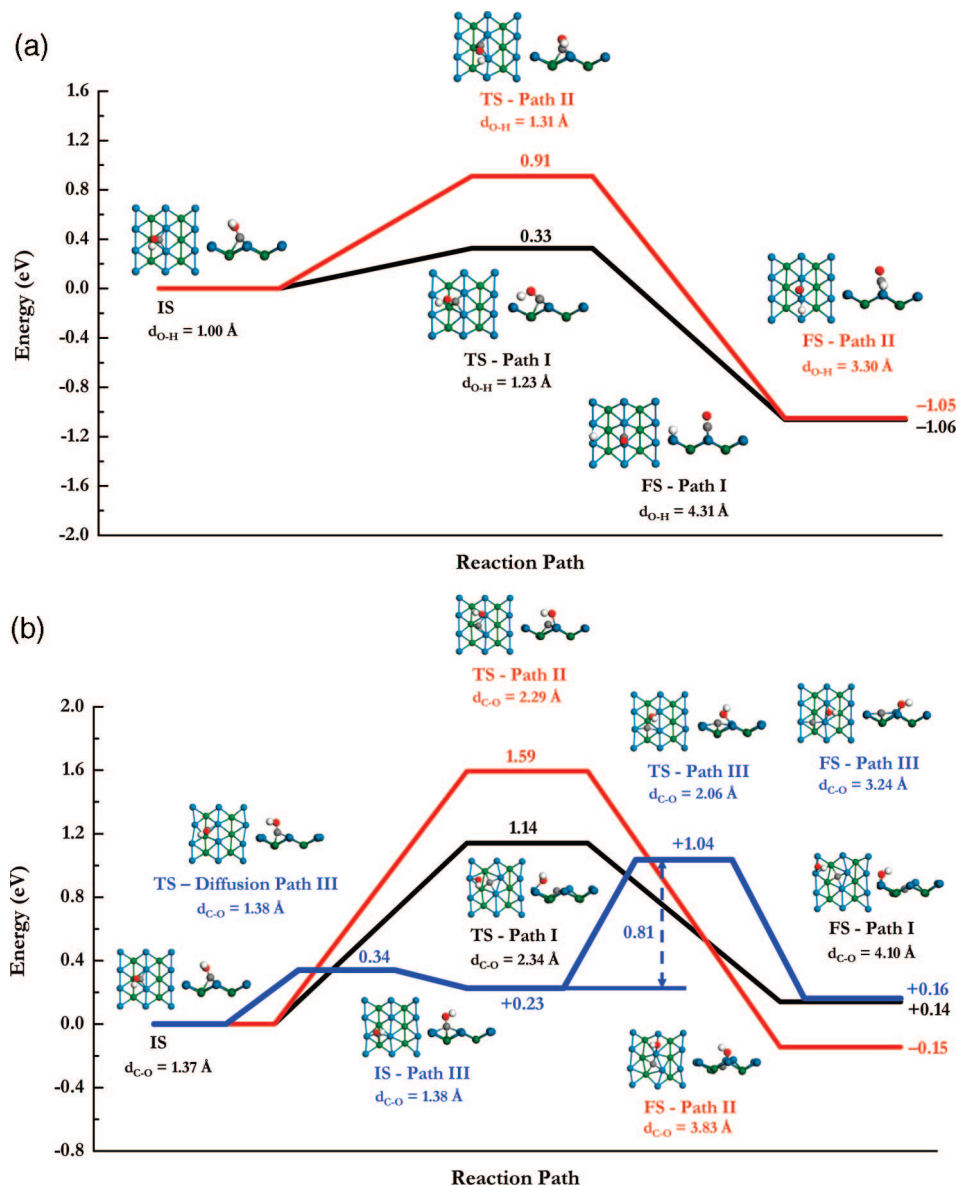
Methanol Decomposition on Cu(110)

J. Phys. Chem. C, Vol. 113, No. 11, 2009 **4533**

Figure 9. Reaction pathways of COH: (a) O−H scission; (b) C−O scission.

Our results suggest that the formation of carbon species on Cu(110) is unlikely, which is consistent with previous experiments.[27]

4. Discussion

Methanol is the simplest molecular form of alcohol. Methanol decomposition is also a good prototype reaction for illustrating the computational method used in this work by showing how many reaction events are possible for even a small molecule on a single-crystal metal surface. Although only partial decomposition of methanol is observed experimentally on Cu(110), we have mapped out a more complete landscape for the decomposition of methanol and its decomposition products. The focus of this work is to demonstrate a method which can be used to automatically determine complex networks of reaction pathways. Different conditions such as temperature, pressure, and the presence of oxygen on the surface could alter the dominant pathway through the network. Figure 10 shows the reaction network of methanol decomposition on Cu(110). The activation barrier and the reaction energy of the pathway with the lowest barrier for each decomposition step are used. It is

clear that adsorbed methanol most favorably proceeds as follows: $CH_3OH \rightarrow CH_3O \rightarrow CH_2O$. Formaldehyde would desorb from the Cu(110) surface rather than continue to dehydrogenate into CO. After the initial O−H bond scission of methanol, three consecutive C−H bond scissions are most likely to occur. The rate-limiting step in this methanol decomposition route is the abstraction of a methylic hydrogen from methoxy; the barrier for C−H bond scission of methoxy to formaldehyde is at least 0.5 eV higher than the other step in this route. This is consistent with experimental observations that methoxy was found as the most abundant surface intermediate on the Cu(110) surface.[7,8,11,28,29] Our results are also in agreement with previous DFT results.[13,14] Sakong and Gross found the barrier for methanol decomposition to methoxy is 0.68 eV, much lower than the barrier of 1.22 eV for methoxy decomposition to formaldehyde.[13] They also suggested that the rate-limiting step in methanol decomposition is the methoxy decomposition into formaldehyde. We also note that the barrier of the reverse process that methoxy recombines with atomic hydrogen forming methanol is 0.92 eV, which is lower than the methoxy decomposition barrier of 1.11 eV. Since the calculated barrier
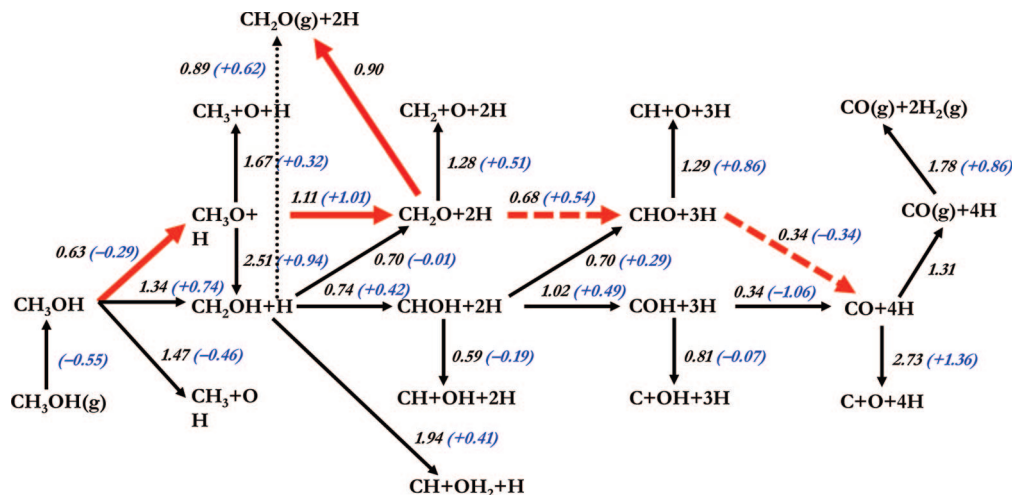
Figure 10. Reaction network of methanol decomposition on Cu(110). The solid and dashed lines denote all the pathways identified in the present work. The lowest activation barrier and the reaction energy (in parenthesis) of each step are listed. Any necessary diffusion barriers are assumed to be low and are not included in these energetics.

for the recombinative desorption of hydrogen is only 0.74 eV, the reverse recombination process of methoxy with hydrogen is limited by the availability of surface atomic hydrogen. As a result, methoxy can further decompose into formaldehyde with the highest barrier among entire decomposition reaction route. A further analysis of the rate constants for elementary steps that will be discussed below confirms this conclusion.

The second methanol decomposition route begins with the initial C−H bond scission of methanol. Following the lowest barrier for each step, the second methanol decomposition route proceeds as

$$CH_3OH \rightarrow CH_2OH \rightarrow CH_2O \text{ (or CHOH)} \rightarrow CHO \rightarrow CO$$
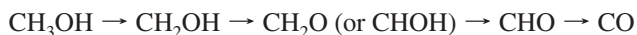
Compared to the most favorable decomposition route, the first step involving methanol dissociation into hydroxymethyl is difficult. Methanol dehydrogenation into hydroxymethyl is the rate-limiting step in this second methanol decomposition route. After the formation of hydroxymethyl, two steps that lead to formaldehyde and hydroxymethylene are competitive with nearly the same activation barriers. We note that surface hydroxymethylene species is unstable because there are three subsequent low-barrier reaction paths, the most favorable being the hydrogenation back into hydroxymethyl. It is worth mentioning that, although hydroxymethyl is unlikely to be formed from methanol decomposition via C−H bond scission, hydroxymethyl could be formed by gas-phase formaldehyde or by hydrogenation (the reverse processes of second route) since the barriers of these steps are small. As shown in Figure 10, the barriers for the reaction from formaldehyde to hydroxymethyl, hydroxymethylene hydrogenation to hydroxymethyl, as well as formyl hydrogenation to hydroxymethylene are 0.27, 0.32, and 0.41 eV, respectively. Therefore, it is important that the complete picture of methanol decomposition on Cu(110) should include the second methanol decomposition route and the corresponding surface intermediate species despite the fact that these species are not clearly identified in the experiments.

The energies listed in Figure 10 do not include zero-point energy effect corrections (ZPECs). Harmonic ZPECs were calculated for all pathways based upon vibrational frequencies of initial, transition, and the final states. It is found that ZPECs do not alter the general trend and conclusions of this work, although they do contribute a small reduction in the activation barrier for each pathway (<0.1 eV).

Although we have focused on the decomposition reaction pathways of each intermediate via one of three possible bond scissions, several other reaction pathways that involve multiple bond-breaking and bond-making processes have also been identified. For example, we have discussed the concurrent C−O and C−H scissions of CH$_2$OH forming CH and H$_2$O in section 3.2.3.3. Another example is that we find a direct conversion between methoxy and hydroxymethyl. The activation barrier of this intermolecular hydrogen transfer reaction is 2.51 eV, and the reaction energy is +0.94 eV. The direct pathway to hydrogen production from hydroxymethylidyne is also identified. The barrier for CHOH ↔ CO + H$_2$(gas) path is 2.97 eV. Since these reaction pathways are kinetically unimportant due to their extremely high barriers, we do not discuss these reaction pathways in detail.

The actual reaction rate constants of the elementary steps depend not only on the magnitude of activation barriers but also on the pre-exponential factors. The reaction rate constant r_i of each path (both forward and reverse) is calculated using harmonic transition state theory[30,31]

$$r_i = v_i \exp\left(\frac{-E_a^\ddagger}{RT}\right) \qquad (2)$$

where v_i is the pre-exponential factor and $E_a^\ddagger$ is the activation barrier. Within harmonic transition state theory, we can calculate the pre-exponential factors (v_i) of each reaction pathway using

$$v_i = \frac{\prod_1^{3N} f_i^{IS}}{\prod_1^{3N-1} f_i^{TS}} \qquad (3)$$

the following definition:
where f_i^{IS} are the vibrational frequencies at the initial state and f_i^{TS} are the vibrational frequencies at the transition (excluding the imaginary one). For the reverse pathway, the f_i^{FS}, which are the vibrational frequencies at the final state, were used instead of f_i^{IS} in eq 3. All calculated pre-exponential factors along with the reaction rate constants for the identified pathways at 300 K are listed in Table 3.
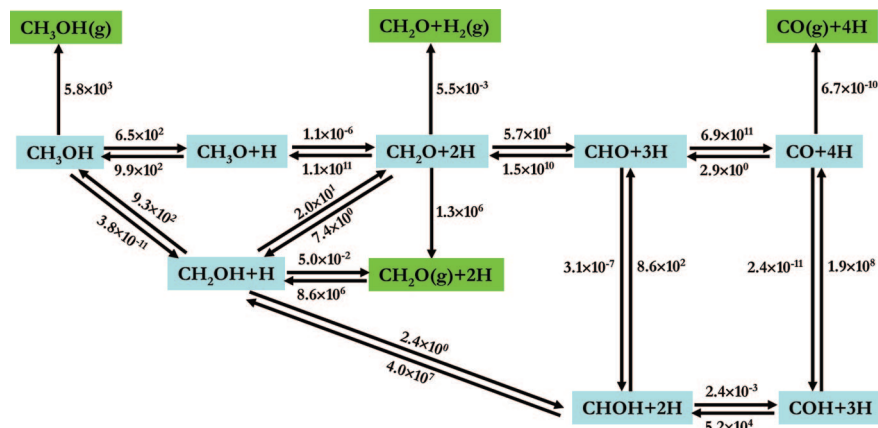
Figure 11. Calculated reaction rate constants for the major elementary steps in methanol decomposition on Cu(110).

TABLE 3: Calculated Activation Barriers $E^{\ddagger}$ (eV), the Pre-exponential Factors v (s^{-1}), and the Rate Constants k (s^{-1}) at 300 K for the Identified Reaction and Diffusion Pathways[a]

reaction paths	v_{forward}	$E^{\ddagger}_{\text{forward}}$	v_{reverse}	$E^{\ddagger}_{\text{reverse}}$	k_{forward}	k_{reverse}
CH$_3$O* H(sb) ↔ CH$_3$O*(sb) + H(sb)	2.38×10^{13}	0.63	2.84×10^{12}	0.92	6.46×10^{2}	9.20×10^{-4}
CH$_3$O*H(top) ↔ CH$_3$O*(top) + H(sb)	1.17×10^{12}	0.86	2.03×10^{13}	0.53	7.22×10^{-2}	9.90×10^{2}
CH$_3$O*H(top) ↔ CH$_3$O*(sb) + H(fcc)	1.19×10^{12}	1.10	5.07×10^{13}	1.28	4.44×10^{-7}	1.53×10^{-8}
CH$_3$O*H(top) ↔ CH$_3$O*(sb) + H(sb)	1.49×10^{13}	1.17	1.47×10^{14}	1.40	2.93×10^{-7}	3.94×10^{-10}
CH$_3$O*H(top) ↔ C* H$_2$OH(sb) + H(sb)	1.40×10^{12}	1.34	1.47×10^{13}	0.61	3.82×10^{-11}	9.34×10^{2}
CH$_3$O*H(top) ↔ C*H$_3$(sb)+ O*H(fcc)	4.87×10^{13}	1.47	1.08×10^{14}	1.94	9.43×10^{-12}	3.22×10^{-19}
CH$_3$O*H(top) ↔ C*H$_3$(sb) + O*H(sb)	1.47×10^{12}	1.74	1.72×10^{13}	2.38	1.05×10^{-17}	1.79×10^{-27}
CH$_3$O*(sb) ↔ CH$_2$O*(sb) + H(sb)	5.48×10^{12}	1.11	6.36×10^{12}	0.10	1.10×10^{-6}	1.14×10^{11}
CH$_3$O*(sb) ↔ C*H$_3$(sb) + O(fcc)	3.47×10^{12}	1.67	1.69×10^{13}	1.35	2.83×10^{-16}	3.13×10^{-10}
CH$_3$O*(sb) ↔ C*H$_3$(sb) + O(fcc)	1.09×10^{13}	2.10	3.93×10^{13}	1.85	5.49×10^{-23}	3.96×10^{-18}
C*H$_2$O*H(sb) ↔ C* H$_2$O*(sb) + H(fcc)	1.03×10^{12}	0.70	5.79×10^{12}	0.71	2.02×10^{1}	7.38×10^{0}
C*H$_2$OH(sb) ↔ C*HOH(sb) + H(sb)	5.61×10^{12}	0.74	8.38×10^{12}	0.32	2.42×10^{0}	3.96×10^{7}
C*H$_2$O*H(lb) ↔ C*H$_2$O*(lb) + H(fcc)	4.14×10^{13}	0.84	4.05×10^{13}	0.86	3.88×10^{-1}	1.24×10^{-1}
C*H$_2$OH(sb) ↔ CH$_2$O(gas) + H(fcc)	3.81×10^{13}	0.89	2.96×10^{11}	0.27	4.96×10^{-2}	8.61×10^{6}
C*H$_2$O*(sb) ↔ C*H$_2$O*(sb) + H(fcc)	1.75×10^{14}	1.19	6.05×10^{13}	1.03	1.53×10^{-6}	3.24×10^{-4}
C*H$_2$OH(sb) ↔ C*H(fcc) + H$_2$O*(top)	1.96×10^{13}	1.94	2.15×10^{12}	1.52	5.63×10^{-20}	5.36×10^{-14}
C*H$_2$O*(lb) ↔ C*HO*(lb) + H(sb)	1.70×10^{13}	0.68	4.34×10^{12}	0.15	5.70×10^{1}	1.47×10^{10}
C*H$_2$O*(sb) ↔ C*HO*(sb) + H(sb)	8.37×10^{12}	0.79	1.17×10^{13}	0.57	4.48×10^{-1}	2.66×10^{3}
C*H$_2$O*(sb) ↔ C*HO*(sb) + H(sb)	2.21×10^{13}	0.95	6.29×10^{12}	0.48	2.51×10^{-3}	5.86×10^{4}
C*H$_2$O*(sb) ↔ C*H$_2$(sb) + O(fcc)	1.86×10^{12}	1.28	7.32×10^{12}	0.78	5.19×10^{-10}	6.22×10^{-1}
C*H$_2$O*(lb) ↔ C*H$_2$(lb) + O(fcc)	2.41×10^{13}	1.82	2.09×10^{13}	1.46	5.92×10^{-18}	5.51×10^{-12}
C*H$_2$O*(sb) ↔ C*H$_2$O*(lb)	2.02×10^{12}	0.47	1.00×10^{13}	0.62	2.38×10^{4}	3.42×10^{2}
C*HO*H(lb) ↔ C*H(lb) + O*H(sb)	5.03×10^{12}	0.44	1.69×10^{13}	0.90	1.89×10^{5}	1.38×10^{-2}
C*HOH(sb) ↔ C*H(fcc) + O*H(sb)	6.92×10^{10}	0.59	8.55×10^{13}	0.78	8.47×10^{0}	7.85×10^{0}
C*HO*H(lb) ↔ C*HO(sb) + H(sb)	5.99×10^{12}	0.59	1.40×10^{13}	1.17	8.56×10^{2}	3.09×10^{-7}
C*HOH(sb) ↔ C*HO(sb) + H(fcc)	8.55×10^{13}	0.70	6.92×10^{10}	0.41	1.73×10^{2}	8.95×10^{3}
C*HOH(top) ↔ C*HO(sb) + H(fcc)	1.26×10^{13}	0.92	1.34×10^{13}	0.57	4.24×10^{-3}	3.05×10^{3}
C*HOH(sb) ↔ C*H(fcc) + O*H(sb)	2.45×10^{13}	0.92	6.70×10^{14}	0.57	8.25×10^{-3}	1.52×10^{5}
C*HOH(sb) ↔ C*H(fcc) + O*H(sb)	3.57×10^{12}	0.97	7.65×10^{12}	1.14	1.74×10^{-4}	5.39×10^{-7}
C*HOH(sb) ↔ C*OH(fcc) + H(fcc)	3.20×10^{13}	1.02	4.89×10^{13}	0.53	2.43×10^{-4}	5.22×10^{4}
C*HOH(sb) ↔ C*OH(fcc) + H(fcc)	3.68×10^{13}	1.14	1.92×10^{13}	0.12	2.80×10^{-6}	1.78×10^{11}
C*HOH(sb) ↔ C*OH(fcc) + H(sb)	7.85×10^{13}	1.36	2.55×10^{13}	0.72	1.03×10^{-9}	2.39×10^{1}
C*HOH(sb) ↔ C*HOH(sb)(rotation)	8.52×10^{12}	0.26	4.53×10^{13}	0.47	3.95×10^{8}	5.53×10^{5}
C*HO(sb) ↔ C*O(sb) + H(sb)	9.95×10^{12}	0.07	1.27×10^{13}	0.75	6.90×10^{11}	2.94×10^{0}
C*HO*(sb) ↔ C*O(sb) + H(sb)	5.86×10^{11}	0.54	3.42×10^{14}	0.86	5.80×10^{2}	1.37×10^{0}
C*HO*(sb) ↔ C*O(top) + H(fcc)	4.71×10^{14}	0.57	2.55×10^{13}	0.77	1.07×10^{5}	3.45×10^{0}

[a] sb, lb, and fcc denote the short-bridge, the long-bridge, and pseudo-fcc(111) sites, respectively.

Figure 11 illustrates the important elementary steps in methanol decomposition on Cu(110). The rate constant of each step listed in Figure 11 is calculated using the pathway with the lowest barrier. Because the diffusion barriers of reaction intermediates are generally small, we assume that the migration of each reaction intermediate from the most stable state to the initial state in the decomposition (or its reverse recombination process) step will not affect the progress of the entire decomposition reaction. The first step for methanol decomposition is methanol dissociates into methoxy via O−H bond scission. Our calculated rate constant for this step is 6.5×10^2 s^{-1}, which is slower than the desorption rate constant of 5.8×10^3 s^{-1} for adsorbed methanol. The adsorbed methanol would rather desorb from the surface than dissociate into methoxy on the clean Cu(110) surface. This is consistent to the experimental TPD results that most adsorbed methanol desorb from the surface with the peak temperature below 200 K and only a small amount of methanol dissociated into methoxy on the clean Cu(110) surface.[7,8,11] The calculated rate constants suggest that the O−H bond scission of methanol is a quasi-equilibrium step since the

forward and the reverse rate constants are very close (6.5×10^2 s^{-1} vs 9.9×10^2 s^{-1}).

The rate-limiting step for methanol decomposition on Cu(110) is the abstraction of a methylic hydrogen (C−H bond scission) of methoxy to produce formaldehyde. The calculated pre-exponential factor and the activation barrier are 5.5×10^{12} s^{-1} and 1.11 eV, respectively. Madix and Telfold studied the primary and second kinetic effects of methoxy dehydrogenation on Cu(110).[29] The pre-exponential factor of $0.8 \pm 0.3 \times 10^{12}$ s^{-1} and the activation energy of 0.91 eV have been reported based on a first-order reaction assumption. Our calculated activation barrier is slightly higher than the experimentally measured barrier, but the pre-exponential factor is also somewhat larger. As a result, our calculated reaction rate constant of 1.1×10^{-6} s^{-1} for methoxy decomposition to formaldehyde is slightly lower than the experimentally measured rate of 4.1×10^{-4} s^{-1}.[29] The formed methoxy can recombine with a neighboring atomic H to yield methanol. Our calculated rate constant for this process is 9.9×10^2 s^{-1}, which is significantly faster than methoxy decomposition to formaldehyde. However, since the recombinative desorption of hydrogen on Cu(110) is faster, the methoxy recombining with the atomic hydrogen forming methanol is limited by the availability of surface atomic hydrogen. This causes the methoxy decomposition step to be even more difficult on the Cu(110) surface. It is well-known that the preadsorbed atomic O on this surface facilitates methanol decomposition.[7,8,11] Surface oxygen atoms not only promote methanol decomposition by directly reacting with incoming gas-phase methanol but also prevent the formation of methanol from the recombination of methoxy and hydrogen by removing surface hydrogen to form water. Previous DFT calculations show that the rate-limiting step is very slightly affected by the presence of surface O atoms. The barrier for methoxy decomposition to formaldehyde is lowered by only 0.14 eV with the assistance of surface oxygen.[14]

Once formaldehyde is formed on Cu(110), it can be consumed through four possible reaction pathways. Formaldehyde can easily desorb from the surface or be hydrogenated into methoxy or hydroxymethyl by recombining with hydrogen or dehydrogenated into formyl via C−H bond scission. The hydrogenation of formaldehyde to methoxy is 10^5 times faster than formaldehyde desorption and will dominate if sufficient atomic hydrogen is available. Our results are consistent with the experimental observations that methoxy is the most abundant and stable species in methanol decomposition on the Cu(110) surface.[7,8,11] Sexton et al. found methoxy is stable until 360−370 K.[11] The other two reaction paths for formaldehyde dehydrogenation to formyl or formaldehyde hydrogenation to hydroxymethyl are slower. As shown in Figure 11, the most favorable route of CH$_3$OH → CH$_3$O → CH$_2$O → CHO → CO, has the dehydrogenation of formaldehyde to formyl as the second slowest step. Even though the step for formyl decomposing into CO is very fast (4.1×10^{-4} s^{-1}), the second bottleneck step that formyl produced from the dehydrogenation of formaldehyde is slow. As such, the CO formation is hindered. Formaldehyde becomes the final product for methanol decomposition on Cu(110). Wachs and Madix studied formaldehyde oxidation on Cu(110) surface. They claimed that almost all formaldehyde molecularly adsorbs on the surface and the Cu(110) surface cannot break the C−H bond to produce formyl.[27] This is the reason why CO is not identified in methanol decomposition experiments on the clean Cu(110) surface.[27]

We have found that gas-phase formaldehyde reacts with surface hydrogen atom, forming hydroxymethyl species on Cu(110). The rate constant of this step is high (8.6×10^6 s^{-1}). Once hydroxymethyl is formed, it is most likely hydrogenated into methanol if adjacent surface atomic hydrogen is available. Except for the favorable hydrogenation path, hydroxymethyl can be dehydrogenated into formaldehyde via O−H bond scission and either release formaldehyde into the gas phase or remain adsorbed to the surface. Based on calculated rate constants, the reaction pathway leading to the adsorbed formaldehyde (2.0×10^1 s^{-1}) is preferred to the release of formaldehyde in the gas phase (5.0×10^{-2} s^{-1}). However, since there is a strong repulsive interaction between coadsorbed formaldehyde and atomic hydrogen, formaldehyde might quickly desorb after the reaction. Hydroxymethyl can also be dehydrogenated into hydroxymethylene via C−H bond scission. However, all above three reaction paths are relatively slow. As a result, neither hydroxymethyl nor hydroxymethylene had been detected on Cu(110) in methanol TPD experiments.

5. Conclusions

The potential energy surface of methanol on the Cu(110) has been explored using periodic DFT calculations combined with the dimer saddle point searching method. Starting from the initial state that stable adsorbed methanol at the short-bridge site on Cu(110), we have identified multiple reaction pathways for each possible bond (O−H, C−H, and C−O) scission process in methanol decomposition. We also calculated the pre-exponential factor of each identified reaction and obtained the reaction rate constant of each identified reaction pathway in the reaction network using harmonic transition state theory. On the basis of calculated rate constants, we found that CH$_3$OH → CH$_3$O → CH$_2$O → CHO → CO is the most favorable route for methanol complete decomposition toward CO on Cu(110). In this complete decomposition route, the formed formaldehyde most likely desorbs from the surface before further dehydrogenation into CO. The rate-limiting step in this route is the dehydrogenation of methoxy to formaldehyde. Our calculations are in agreement with the reported experimental data and observations, and most importantly, we demonstrated that the computational methodology used in this work provides a powerful tool to investigate complex heterogeneous catalytic reaction mechanisms.

References and Notes

(1) Henkelman, G.; Jonsson, H. *J. Chem. Phys.* **1999**, *111*, 7010.
(2) Mei, D.; Xu, L.; Henkelman, G. *J. Catal.* **2008**, *258*, 44.
(3) Olsen, R. A.; Kroes, G. J.; Henkelman, G.; Arnaldsson, A.; Jonsson, H. *J. Chem. Phys.* **2004**, *121*, 9776.
(4) Xu, L. J.; Henkelman, G. *J. Chem. Phys.* **2008**, *129*, 114104.
(5) Palo, D. R.; Dagle, R. A.; Holladay, J. D. *Chem. Rev.* **2007**, *107*, 3992.

(6) Rozovskii, A. Y.; Lin, G. I. *Top. Catal.* **2003**, *22*, 137.

(7) Wachs, I. E.; Madix, R. J. *J. Catal.* **1978**, *53*, 208.

(8) Bowker, M.; Madix, R. J. *Surf. Sci.* **1980**, *95*, 190.

(9) Russell, J. N.; Gates, S. M.; Yates, J. T. *Surf. Sci.* **1985**, *163*, 516.

(10) Sexton, B. A. *Surf. Sci.* **1979**, *88*, 299.

(11) Sexton, B. A.; Hughes, A. E.; Avery, N. R. *Surf. Sci.* **1985**, *155*, 366.

(12) Sakong, S.; Gross, A. *J. Catal.* **2005**, *231*, 420.

(13) Sakong, S.; Gross, A. *J. Phys. Chem. A* **2007**, *111*, 8814.

(14) Sakong, S.; Sendner, C.; Gross, A. *J. Mol. Struct.: THEOCHEM* **2006**, *771*, 117.

(15) Greeley, J.; Mavrikakis, M. *J. Catal.* **2002**, *208*, 291.

(16) Blochl, P. E. *Phys. Rev. B* **1994**, *50*, 17953.

(17) Kresse, G.; Joubert, D. *Phys. Rev. B* **1999**, *59*, 1758.

(18) Perdew, J. P.; Wang, Y. *Phys. Rev. B* **1992**, *45*, 13244.

(19) Kresse, G.; Furthmuller, J. *Phys. Rev. B* **1996**, *54*, 11169.

(20) Kresse, G.; Furthmuller, J. *Comput. Mater. Sci.* **1996**, *6*, 15.

(21) Bader, M.; Puschmann, A.; Haase, J. *Phys. Rev. B* **1986**, *33*, 7336.

(22) Desai, S. K.; Neurock, M.; Kourtakis, K. *J. Phys. Chem. B* **2002**, *106*, 2559.

(23) Greeley, J.; Mavrikakis, M. *J. Am. Chem. Soc.* **2002**, *124*, 7193.

(24) Greeley, J.; Mavrikakis, M. *J. Am. Chem. Soc.* **2004**, *126*, 3910.

(25) Janik, M. J.; Taylor, C. D.; Neurock, M. *Top. Catal.* **2007**, *46*, 306.

(26) Gomes, J. R. B.; Gomes, J. *J. Electroanal. Chem.* **2000**, *483*, 180.

(27) Wachs, I. E.; Madix, R. J. *Surf. Sci.* **1979**, *84*, 375.

(28) Barnes, C.; Pudney, P.; Guo, Q. M.; Bowker, M. *J. Chem. Soc., Faraday Trans.* **1990**, *86*, 2693.

(29) Madix, R. J.; Telford, S. G. *Surf. Sci.* **1995**, *328*, L576.

(30) Vineyard, G. H. *J. Phys. Chem. Solids* **1957**, *3*, 121.

(31) Wert, C.; Zener, C. *Phys. Rev.* **1949**, *76*, 1169.